FULL PAPER

Conducting Domain Walls in Lithium Niobate Single Crystals

*Mathias Schröder, Alexander Haußmann, Andreas Thiessen, Elisabeth Soergel, Theo Woike, and Lukas M. Eng**

Ferroic materials play an increasingly important role in novel (nano)electronic devices. Recently, research on domain walls (DWs) receives a big boost by the discovery of DW conductivity (DWC) in $BiFeO_3$ and $Pb(Zr_xTi_{1-x})O_3$ ferroic thin films. Here, it is demonstrated that DWC is not restricted to thin films, but equally applies to millimeter-thick wide-bandgap, ferroic single crystals, such as $LiNbO_3$. In this material transport along DWs can be switched by super-bandgap illumination and tuned by engineering the tilting angle of DWs with respect to the polar axis. The results are consistently obtained using conductive atomic force microscopy to locally map the DWC and macroscopic contacts, thereby in addition investigating the temperature dependence, DW transport activation energies, and relaxation behavior.

1. Introduction

Ferroic materials have proven to play a vital role in novel electronic devices, among which non-volatile ferroelectric random access memories (FeRAM) are probably most prominent.[1] When using structured ferroics[2] that possess distinct domain patterns, the number of possible applications increases tremendously; periodically poled lithium niobate ($LiNbO_3$: LNO) non-linear optical crystals for efficient frequency conversion[3] or densely arranged nanometer-sized domains for utmost density data storage[4] are just two prominent examples to be mentioned.

These beautiful examples, however, rely solely on the properties of ferroelectric domains as a whole, making clever use of the change of spontaneous polarization P_S from domain to domain. Only recently, ferroic domain walls (DWs) were brought into focus, not only from the academic point of view because of constituting highly confined regions with different dielectric behavior,[5] but moreover also for their spectacular possibilities in applications.[6] Despite their tiny width of sub-to-few nanometers only,[7–9] DWs strongly affect the electronic, magnetic, mechanical, or optical material properties on different length scales, a) clearly due to local symmetry breaking, but b) equally in the overall macroscopic sample performance such as the dielectric behavior.[10] For instance the assembly of nanowires by means of ferroelectric lithography (using DW decoration) was successful only due to the local DW-specific variation of the surface chemistry.[11,12]

In particular, the electrical conductivity of ferroelectric DWs has captured huge interest for the last years, as this opens a realistic and unique perspective to reproducibly engineer conductive paths and nanocontacts of sub-nanometer dimension into wide-bandgap materials. Taking control over and being able to purposely induce and govern conductive DWs in insulating templates thus is key for the applicability in novel nanoelectronic devices.

The very first evidences for ionic and/or electronic transport along DWs were pointed out in the pioneering work of E. Saljé in ferroelastic $CaTiO_3$[13] and WO_3.[14,15] More recently, DW conductivity (DWC) in thin films of rhombohedral multiferroic and magneto-electric bismuth ferrite ($BiFeO_3$, BFO) has been investigated experimentally: Both 109° and 180° DWs in BFO behave ohmic as attributed to either electrostatic potential steps or the decrease of the bandgap at DWs,[16] while 71° DWs in the same material show a diode-like behavior stemming from oxygen vacancies at DWs that lower the Schottky barrier.[17] Conduction along 109° DWs in La doped BFO was reported to be thermally induced as explained through electron hopping along oxygen vacancies.[18] Moreover, DWC was also found along 180° DWs in tetragonal lead-zirconate-titanate (PZT) thin films[19] said to originate from oxygen vacancies within DWs as well. It is believed that these DWC issues equally impact on the rather unusual photovoltaic properties of BFO thin films; those findings reported on large photovoltages (way above the bandgap voltage) and photovoltaic currents that propagate perpendicularly to the spontaneous polarization.[20,21] Manifestly, DWC in various DW configurations and in very different ferroelectric thin film materials is clearly evidenced experimentally, backed up with a manifold of possible theoretical explanations. DWC was theoretically proposed to occur also for single crystalline

M. Schröder, Dr. A. Haußmann, A. Thiessen, Prof. L. M. Eng
Institute of Applied Photophysics
TU Dresden
George-Bähr-Str. 1, 01062 Dresden, Germany
E-mail: lukas.eng@iapp.de
Dr. E. Soergel
Institute of Physics
University of Bonn
Wegelerstraße 8, 53115 Bonn, Germany
Dr. T. Woike
Institute of Structural Physics of Condensed Matter
TU Dresden
Zellescher Weg 16, 01062 Dresden, Germany

DOI: 10.1002/adfm.201201174

materials.[22,23] First experimental evidence for this was obtained on erbium manganite ($ErMnO_3$)[24] as well as holmium manganite ($HoMnO_3$).[25] These materials are termed "improper ferroelectrics", since ferroelectricity is not the primary order parameter. Due to this, the DWs are curved and form all possible orientations with respect to the fixed polar axis along their paths. In both cases, negatively charged tail-to-tail regions of a DW showed an enhanced conductivity compared to the bulk, whereas at the positively charged head-to-head sections the conductivity was suppressed.

However, in $ErMnO_3$ and $HoMnO_3$ DWC was measured on natural domain structures without the attempt to control, engineer or switch the currents on the DW. To fill this gap we show here experimentally that (so-called) 180° DWs in bulk LNO single crystals (sc-LNO) have the potential to serve as perfect nanocontacts; they can be engineered into bulk LNO wafers of >0.5 mm thickness with nanometer precision and be used to macroscopically contact nano-objects for a wealth of applications in nanoscience and nanotechnology. Moreover, they can be switched on/off and tuned by the assistance of suitable photons. Finally, we also find them to behave either ohmic or Schottky diode-like depending on the external conditions. In order to gain a deeper insight into the transport mechanism along the DWs, we successfully combined the nanoscopic characterizations (conductive AFM) with macroscopic measurements at various temperatures, allowing for the determination of activation energies.

2. Experimental Setup

2.1. Samples

LNO is known as a perfectly insulating wide-bandgap ($\Delta E \approx 4$ eV) ferroelectric allowing for antiparallel domain splitting only. The 180° DWs are uncharged in equilibrated sc-LNO and align parallel to the polar z-axis.[26] Effectively, DWs in LNO created by electric field poling are found to be slightly inclined with respect to the z axis, with the inclination angle α depending on the specific poling and further annealing procedures. In fact DWs in z-cut LNO can become perfectly non-charged (i.e., $\alpha = 0°$) during moderate heating after electrical poling. On the other hand, a radical heat-treatment close to the Curie temperature allows fabricating a stable head-to-head domain configuration in LNO (with $\alpha \approx 90°$) having exactly one charged DW.[27]

For any inclination angle $\alpha \neq 0$, the DW is charged, therefore exhibiting an interface charge density σ of

$$\sigma = 2 P_s \sin\alpha \quad (1)$$

With respect to α we distinguish between the following DW configurations in LNO (**Figure 1**a):

1) A-LNO: neutral uncharged DWs ($\alpha = 0°$);
2) B-LNO: partially charged DWs ($0° < |\alpha| < 90°$)
3) C-LNO: maximum charged DWs ($|\alpha| \approx 90°$).

We will refer to the corresponding samples as A-LNO, B-LNO, and C-LNO samples, respectively. We are able to reproducibly fabricate all three types of DWs in commercially available flat (< 0.5 nm rms) LNO single crystal wafers up to thicknesses of 0.5 mm. We show that not only the size and position of the DWs, but also the angle α and thus the DW interface charge σ can be controlled precisely. In the present report we restrict ourselves to DWs that have a positive interface charge ($\sigma > 0$).

We also prepared S-LNO samples differing from the above three types in exhibiting surface or spike domains which consequently never penetrate through the full crystal thickness (Figure 1a). Note that the angle α in B-LNO and S-LNO is similar and so is their interface charge density σ.

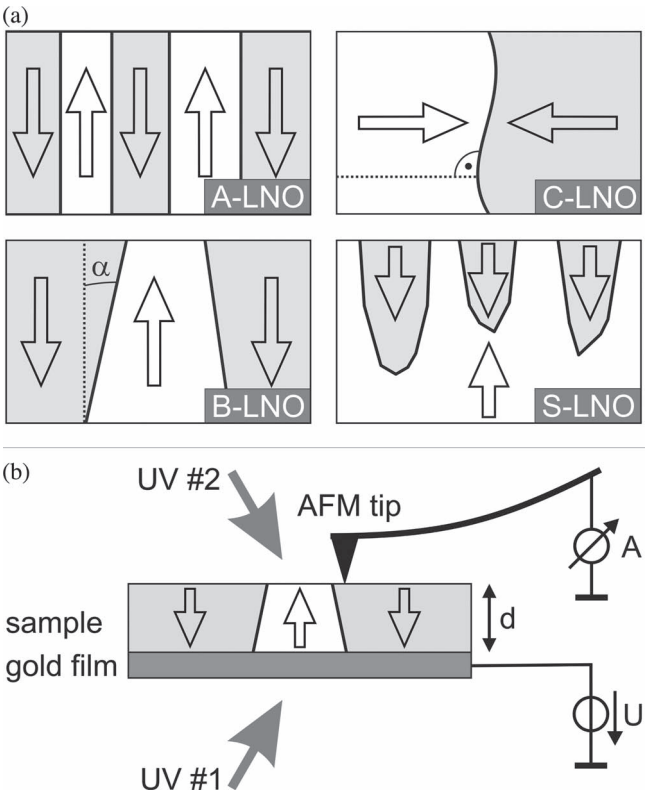

Figure 1. Classification of the investigated DWs and experimental setup. a) Straight 180° DWs perpendicular to the z-surface (A-LNO, $\alpha = 0°$), partially charged DWs (B-LNO, $0° < |\alpha| < 90°$), single and maximum charged DW (C-LNO, $\alpha \approx 90°$), and surface domains (S-LNO, $0° < |\alpha| < 90°$). The direction of the arrows corresponds to the spontaneous polarization and the crystallographic c-axis. b) Experimental setup for the c-AFM investigations exemplified for a B-LNO sample (d: crystal thickness).

2.2. Methods and Experimental Setup

Investigations of the DWC for the 4 types of sc-LNO samples were performed both nano- and macroscopically. The local-scale inspections were carried out with conductive atomic force microscopy (c-AFM) measuring the transport properties along DWs when applying a voltage between a Pt-coated tip and a semi-transparent Cr/Au rear-electrode (Figure 1b). c-AFM measurements were always compared to previously recorded piezoresponse force microscopy (PFM) images, revealing the

effective domain distribution.[28,29] For the macroscopic experiments, ultra-thin semi-transparent Cr/Au electrodes of 2.3 mm diameter were evaporated also onto the top LNO surface, thus constituting a large top electrode that connects both domains and possible DWs in the LNO sample. A single domain LNO sample cut from the same wafer batch always served as a reference sample, allowing to separate the DW contribution from possible currents due to bulk conductivity in these measurements (for details see Supporting Information 1).

For both the nano- and macroscopic experiments, electrical transport along the DWs was also investigated under super- and sub-bandgap illumination, with the goal to induce photocarriers most preferentially within DWs. Bandgap wavelengths are commonly defined in literature using a threshold for the absorptivity (2 mm^{-1}), leading to values in the range of 310 – 320 nm depending on the doping concentration in the LNO.[30] Shorter wavelengths are strongly absorbed within typical penetration depths between 40 μm (λ = 300 nm, 5% Mg doping) and 20 nm (λ = 240 nm).[31] Since our sc-LNO samples measure several 100 μm in thickness d, photocarriers are generated at the sample surface only, while the LNO interior "sees" no photons. Hence we inspected the transport properties in two different configurations (Figure 1b)[32] illuminating the samples either from the bottom (path UV#1) or the top interface (path UV#2).

3. Results

3.1. Local c-AFM Measurements

3.1.1. Conductive Domain Walls

We start our systematic investigation of the DWC with a d = 300 μm thick A-LNO sample using a commercially available congruent, undoped LNO crystal. Neither c-AFM nor the following macroscopic measurements indicated any DWC at ambient conditions, irrespective of the applied bias voltage U (–10 to +10 V) or any additional UV illumination (λ = 250–400 nm).

DWC, however, could be observed in B-LNO samples under super-bandgap illumination. The PFM image in **Figure 2**a illustrates the typical, hexagonal domain configuration obtained in a 5% Mg doped B-LNO sample after electric field poling. Bright and dark areas correspond to c^- - and c^+ - domains with P_S pointing into and out of the sample, respectively. c-AFM images from the same area showed no specific conductivity across the ± 10 V bias range allowing to specify the relevant background peak-to-peak dark-noise current to be ± 200 fA_{pp}. Notably, with additional super-bandgap light at λ = 310 nm (I = 12.5 μW mm^{-2}) a photoinduced DW current up to ~1.4 pA at a +10 V bias can be observed (Figure 2b). The current could be increased to > 50 pA by thinning the B-LNO sample down to 15 μm (for details see Supporting Information 2). Note that upon UV illumination, also the conductivity of the domain areas increases slightly; nevertheless, the measured ≈400 fA domain current is more than one order of magnitude smaller as compared to the reported DW current. We will further refer to this background effect as "bulk current".

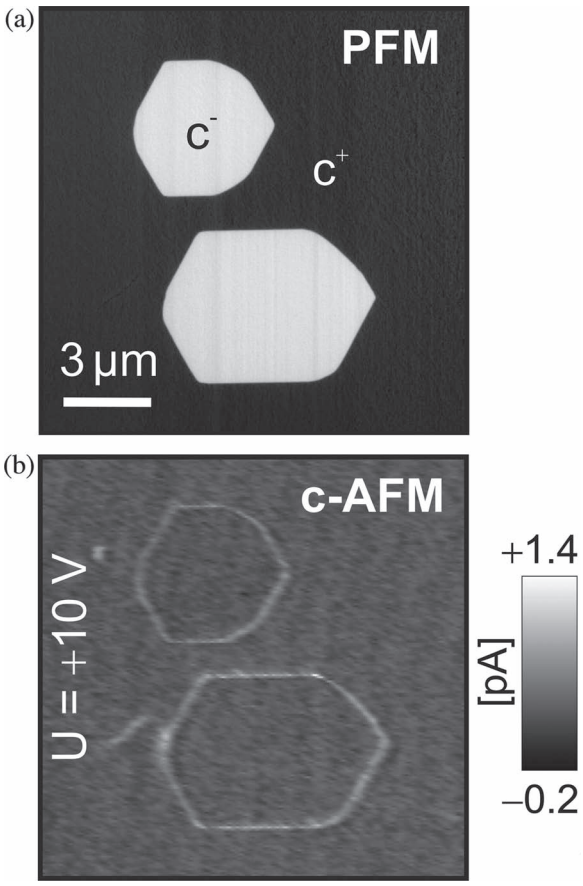

Figure 2. Local measurements on conductive DWs. a) PFM image showing c^+ and c^- domains. b) c-AFM image recorded with super-bandgap illumination (λ = 310 nm, I = 12.5 μW mm^{-2}) via path #2 as shown in Figure 1b.

PFM measurements before and after the c-AFM scans showed no change in the domain position, size and shape within the experimental resolution. This means that the DW remains fixed at its position and no currents from ferroelectric switching are measured during the c-AFM scan.

Two control experiments were carried out in order to verify that the reported currents are really connected to DWC along DWs that fully penetrate through the sc-LNO: i) we compared DWC for bulk and surface domains, i.e. we inspected both B-LNO and S-LNO samples (Figure 1a) and ii) we altered between top and bottom illumination (paths UV#2 and UV#1) in order to vary the location of photoinduced charge carriers with respect to the tip (Figure 1b).

When comparing B-LNO and S-LNO samples by c-AFM (issue (i)) we find DWC to occur for bulk domains in B-LNO only; this underlines that the DWs need to be electrically contacted to the bottom electrode in order to be usable as nanoscale vias (for details see Supporting Information 3). This result implies that charge carrier injection from the bottom electrode is crucial for DWC, as it is expected for conductive channels embedded in an insulating host. With respect to issue (ii) our c-AFM measurements showed the same DW current irrespective of the illumination path. Combining these results, we have demonstrated

that a) the current indeed flows within DWs and b) that these DWs need to penetrate through the whole sample from the bottom to the top interface. Only a very weak leakage current flows through the domain areas due to bulk photoconductivity. Though at larger scan ranges (such as shown in Figure 2b) the DW current signal seems to be rather broad (several 100 nm), higher resolved images showed a distinct confinement of the current to the DWs (well below 100 nm, about twice the tip radius). Obviously, these DWs can be regarded as highly conductive singularities of a very confined width crossing a completely insulating host material!

3.1.2. Dependences of Domain Wall Conductance

DWs in sc-LNO hence constitute excellent nanocontacts. In order to quantify the DWC transport properties with respect to future technological applications we performed a series of local scale and macroscopic experiments. The local scale DWC analysis using c-AFM focused on the following parameters: a)illumination irradiance I and wavelength λ; b) bias voltage U; and c) inclination angle α in B-LNO samples.

Figure 3a displays our c-AFM measurements when varying the UV intensity I = 1–7 μW mm^{-2} while keeping both the wavelength (λ = 270 nm) and bias voltage (U = +10 V) fixed. The DW current is found to increase linearly with the intensity, whereas the current stays constant (within error bars) when recorded from domain areas.

To investigate the DWC as a function of λ, we choose I = 0.5 μW mm^{-2} and the bias voltage (U = +10 V), while varying λ from super-bandgap (240–310 nm) to sub-bandgap (310–400 nm) illumination. Again the current was measured both at the domain areas and the DWs, as illustrated in Figure 3b. As shown, DWC is not measurable for sub-bandgap illumination, reaches a maximum for UV illumination around 300 nm (slightly below the LNO bandgap), and decreases for shorter wavelengths. The current measured from domain areas shows the very same wavelengths dependence, however, reaching at its maximum (λ = 300 nm) an amplitude that is two orders of magnitude smaller when compared to the DWC.

We next investigated the effect of bias voltage polarity on the DWC. Most interestingly, we observe a linear dependence of the DW current for positive sample voltages while no or little current flows in the opposite direction (for details see Supporting Information 4). This suggests the DW to behave diode-like, at least for illumination wavelengths ≤ 300 nm. For illumination at λ = 310 nm, ohmic characteristics were observed. Remarkably, the same ohmic behavior was measured in all our macroscopic experiments, independent of illumination wavelength (see later). Since different electrode materials were used in these investigations (Pt-coated tip and Cr/Au bottom electrode in c-AFM, two identical Cr/Au electrodes for macroscopic characterization), we can conclude that the diode characteristics arise from a Schottky barrier formed by the Pt coated tip and the LNO surface, however, for certain illumination conditions ($\lambda \leq$ 300 nm) only.

The impact of the inclination angle α on the DWC is summarized in **Table 1**. As shown, the larger is α (implying larger values of σ according to Equation 1), the larger is the measured DW current. A maximum current of 13.6 pA was recorded for

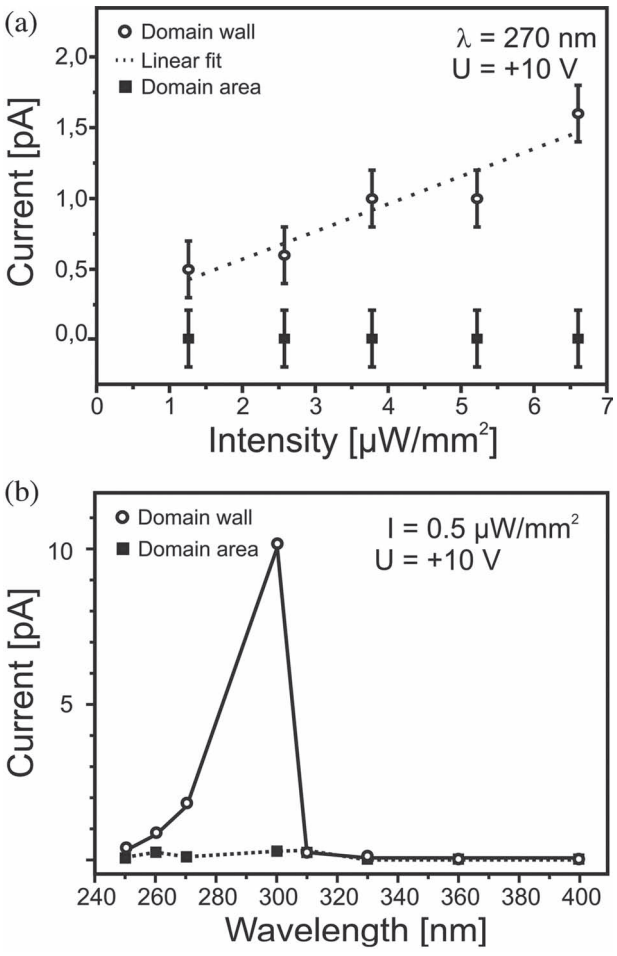

Figure 3. Dependence of the DW current on the external illumination (c-AFM). a) Dependence of DW and domain area current on the illumination intensity at a fixed bias voltage and wavelength. A linear increase of the current at the DWs is recorded. b) Dependence of the DW and domain area current at a fixed bias voltage and intensity. Illumination slightly below the bandgap (λ = 300 nm) yielded highest DW currents and a contrast ratio (= $I_{DW}/I_{domain\ area}$) of ≈100.

α = 0.225°. The crystal forms only slightly inclined DWs during our poling procedure ($\alpha > 0$, $\alpha < 1°$). Furthermore, it is important to note that the DWC does not depend on the Mg content within the LNO crystals; Mg ions though have an influence on the domain shapes and thus on α in the as-poled state (for details see Supporting Information 5).

Table 1 implies that DWC should reach its maximum for α = 90°, the highest possible tilt angle. In fact we succeeded in manufacturing such a C-LNO sample with the results shown in **Figure 4**. The in-plane PFM[33] image in Figure 4a demonstrates that the zigzagged DW clearly separates the two head-to-head polarization directions. Correspondingly, Figure 4b displays the photoinduced DW current as recorded by c-AFM under super-bandgap illumination. Again, the confinement of the current to the DWs is clearly visible, with the current reaching peak values of ≈ ±1 pA in each bias polarity direction. Compared to B-LNO samples (see Table 1), these currents are unexpectedly small.

Table 1. Dependence of the DW current on the Mg content and the inclination of the DW. Variously doped B-LNO samples were analyzed with respect to their DW inclination angle α in the as-poled and annealed state. DW currents were measured at $U = +10$ V under illumination with an intensity of $I = 12.5$ µW mm^{-2} at $\lambda = 310$ nm. As seen, the conductivity directly correlates to α with the exception of $\alpha \approx 90°$. For comparison of differently thick samples, the current was normalized to a thickness of 500 µm as reported in the last column.

Inclination α [°]	Mg content [mol%]	Thickness d [µm]	Current I [pA]	Normalized current [pA per 500 µm^{-1}]
0.006	0	300	< 0.3	< 0.2
0.006	1	500	< 0.2	< 0.2
0.016	5 (annealed)	300	< 0.2	< 0.3
0.024	2	500	0.2	0.2
0.050	3	500	0.4	0.4
0.074	5 (annealed)	300	2.1	3.5
0.225	5	300	13.6	22.7
≈90	0	2000	2.0	8.0

We believe that this is due to the extreme thermal treatment the C-LNO samples underwent during sample preparation.

3.2. Macroscopic Measurements

3.2.1. Conductive Domain Walls

Macroscopic transport experiments are our second experimental mainstay for the analysis of DWC in sc-LNO. They allow accessing a complementary set of parameters as compared to c-AFM. Note, however, that owing to the relatively large electrode areas (up to 4 mm^2) in these experiments, several DWs are contacted simultaneously resulting in much larger DW currents than what was observed by c –AFM. With such macroscopic measurements performed over a broad temperature range we were able to a) record I–U characteristics from DWs, b) analyze the impact of temperature on the DW current, i.e., the activation energies needed for electronic transport along DWs, and c) investigate the DWC transient behavior when switching the UV-light on and off.

Figure 5a displays the current dependence on illumination intensity I at both a fixed wavelength ($\lambda = 300$ nm) and bias voltage ($U = +10$ V). As seen the current measured on a B-LNO sample is ≈7 times larger as compared to the single domain reference sample, a result that we attribute to the DWC. Note that in consistence with the c-AFM experiments, no DWC was measured in the dark. While the single domain current increases linearly with intensity, the B-LNO sample follows a sub-linear power law. These characteristics meet the well-known charge transport model in LNO based on doping and/or defects: while the one-center model shows a linear increase of conductivity vs. illumination intensity, the two- or multi-center model follows a sub-linear behavior[34].

3.2.2. I-U-characteristics

Macroscopic I–U-characteristics recorded on the B-LNO sample are shown in Figure 5b. We observe a linear dependence for both the B-LNO and the reference sample, however, with the latter having a much smaller slope, i.e., conductance. We conclude that photoinduced DWC in LNO must obey an ohmic behavior. Please recall at this stage that our c-AFM measurements with a different top electrode material and configuration (Pt coated tip vs. Cr/Au thin film) showed a Schottky-diode-like characteristic for this wavelength ($\lambda = 300$ nm). Hence, when selecting suitable electrode materials, the DW transport can be switched from bi-directional (ohmic) to Schottky-type transport. Up to now, a full explanation for this effect cannot be given since detailed data for the band structure of Mg doped congruent LNO are not available, and furthermore the influence of charged DWs as well as super-bandgap light on the energy levels are unknown. Nonetheless, the macroscopic data clearly show that the photoinduced DWC allows for full bi-directional transport. We are convinced that the true nature of this effect is reflected best in these measurements, since identical electrodes, a homogeneous electric driving field and no mechanical load such as the contact force exerted by an c-AFM tip are applied.

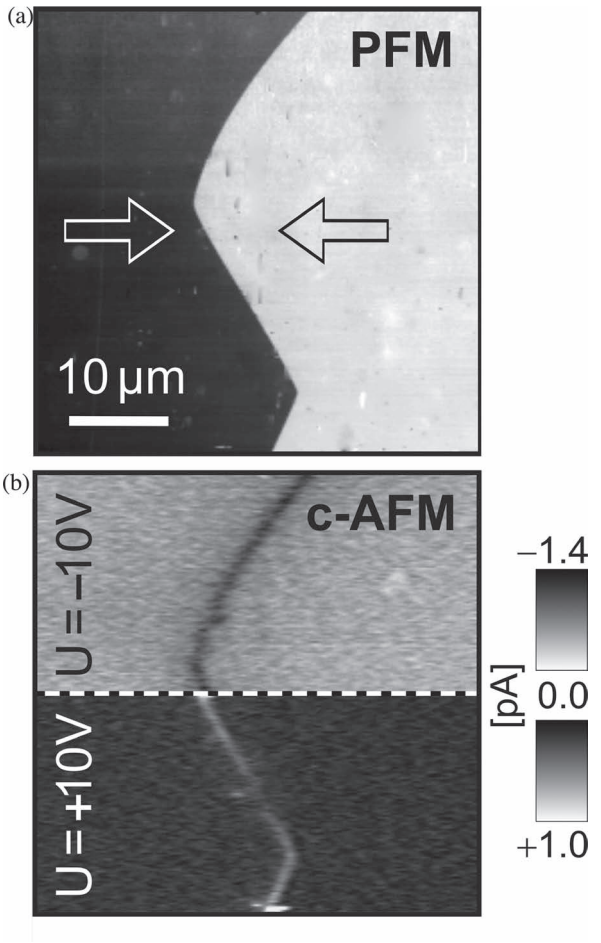

Figure 4. Investigation of a maximum charged DW. a) PFM image taken at the $\alpha \approx 90°$ head-to-head DW (C-LNO sample). The arrows indicate the orientation of the polarization within the domains. b) Combination of two separate c-AFM scans from the same area recorded with opposite applied voltages of –10 V (upper part) and +10 V (lower part) and UV illumination ($\lambda = 310$ nm, $I = 12.5$ µW mm^{-2}) via path #2 as shown in Figure 1b.

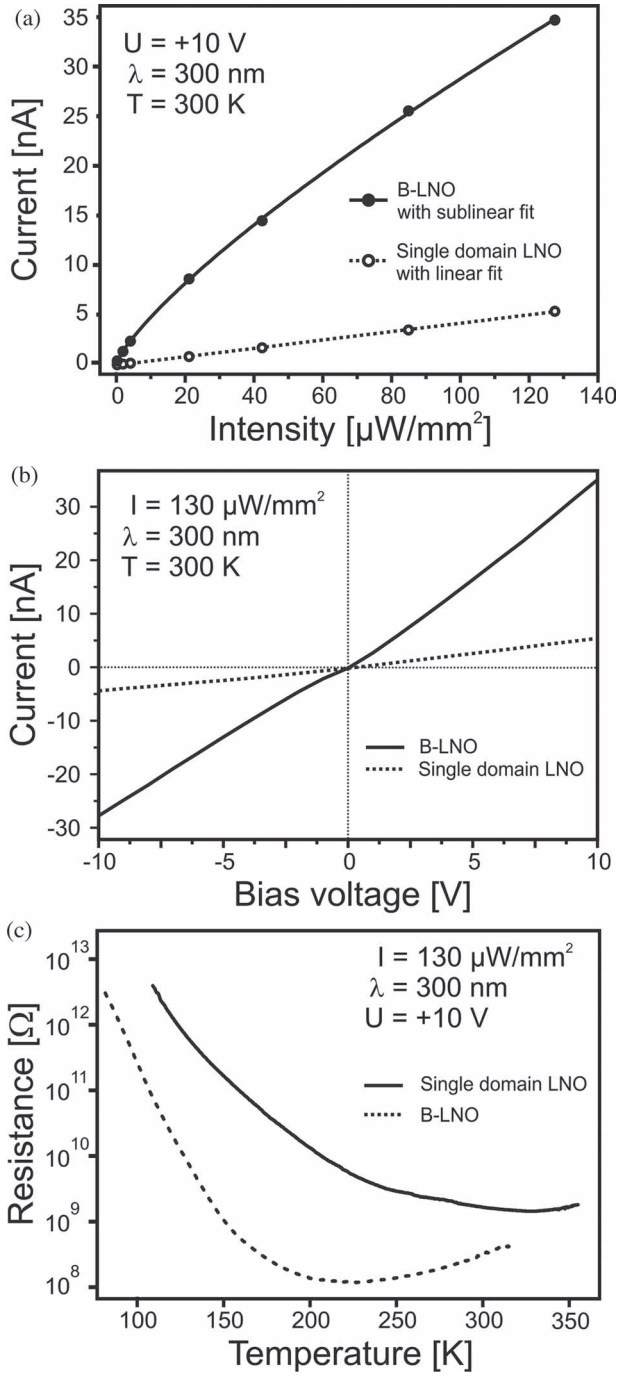

Figure 5. Comparative macroscopic measurements under super-bandgap illumination for single domain and B-LNO. a) Intensity dependence of the current, b) *I-U*-curves at room-temperature, and c) temperature dependence of the resistance.

3.2.3. Temperature Dependence

Figure 5c displays the temperature dependent resistance under super-bandgap illumination for B–LNO and the single domain reference sample between 90–350 K. Obviously, the DW current dominates by one order of magnitude over the current measured through domain areas. At low temperatures, the resistance of both samples decreases with increasing temperature. Such a thermally activated conductivity is best described by the Arrhenius-type equation:

$$R(T) = a \cdot T^{2/3} \cdot \exp\left(\frac{E_a}{k_B T}\right) \quad (2)$$

with E_a the activation energy, T the temperature, k_B the Boltzmann constant and a the proportionality factor. Fitting Equation (2) to our experimental data in Figure 5c reveals activation energies of 100–130 meV (see **Table 2**). Since B-LNO conductivity clearly stems from DWs, we can conclude that at low temperatures the activation energies for bulk and DW conductivity are almost the same. Although E_a is quite similar for the two cases, the two curves clearly differentiate with respect to their minimal resistivity. The minimum is found at 225 K and 330 K for the B-LNO and single domain LNO, respectively, using identical illumination conditions.

3.2.4. Relaxation

Finally, we investigated also the time-dependent DW current evolution: The resistance of a B-LNO sample was recorded while switching the UV illumination on and off, as shown in **Figure 6**a. As seen, the resistance drops by more than 4 orders of magnitude within <2 s when turning on the UV light (the temporal resolution is limited by the experimental setup), whereas the relaxation in the dark proceeds over more than one hour. Note that this result is in full accordance with our c-AFM measurements that yielded a similar transient behavior, although the resistance could not be traced for more than ~15 min due to the noise limit of the current amplifier.

A spread of the data displaying the first ten minutes after switch-off is illustrated in Figure 6b, comparing the B-LNO and the single domain sample (displayed here as the conductance, i.e., inverse resistance). Both sets of data are easily fitted by a stretched exponential function (Kohlrausch-Williams-Watts (KWW) equation)[35,36] following

$$G(t) = (G_1 - G_0) \cdot \exp\left(-\left(\frac{t}{\tau}\right)^{\beta}\right) + G_0 \quad (3)$$

with G_1 and G_0 being the conductance with and without illumination, respectively. For B-LNO, we find $\tau = 7.6 \times 10^{-4}$ s and $\beta = 0.15$, in contrast to $\tau = 1.7 \times 10^{-4}$ s and $\beta = 0.16$ for the single domain LNO sample. It is due to these remarkably small β values that we are able to track the relaxation up to $10^6\tau$.

Table 2. Activation energies for different LNO samples in different temperature regimes.

Sample	Temperature regime [K]	Activation energy *E* [meV]
Single domain LNO	324–243	106 ± 1
B-LNO	190–160	127 ± 1

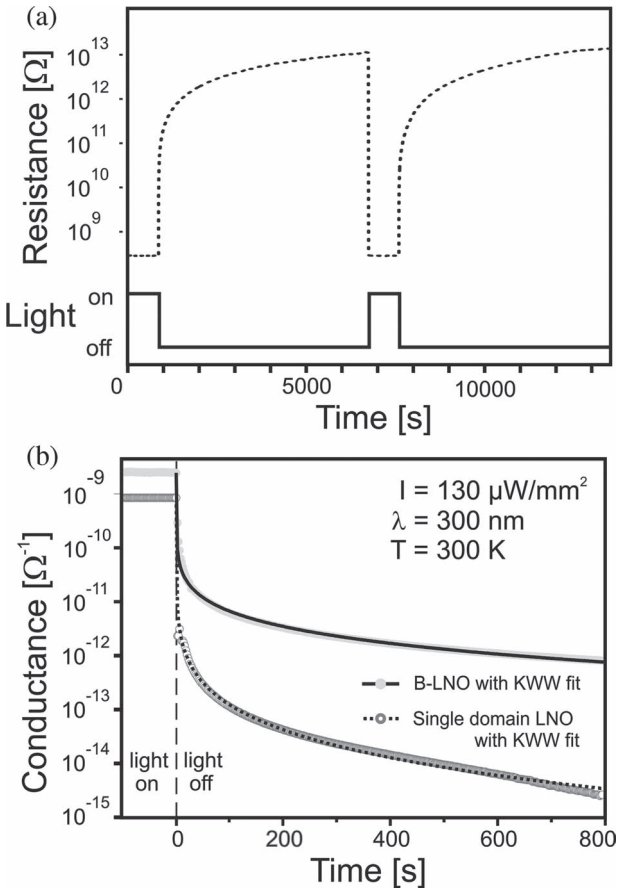

Figure 6. Relaxation behavior of B-LNO. a) Transient response of the resistance in B-LNO at room temperature under constant bias when switching the super-bandgap illumination on and off. b) Conductance relaxation after the illumination is blocked for single domain and B-LNO. Both data sets can be fitted by the Kohlrausch-Williams-Watts (KWW) function.

4. Discussion

When recapitulating our nanoscopic and macroscopic measurements, we can work out the following picture of photoinduced DWC in sc-LNO:

In A-LNO, DWs are neutral ($\alpha = 0°$), no DW current was detected and only a weak bulk conductivity occurred. Obviously, inclined DWs are mandatory for DWC, yielding in our case always a positive interface charge in the investigated B-LNO ($0° < \alpha < 1°$) and C-LNO ($\alpha \approx 90°$) samples. The interface charges attract moveable charge carriers from the bulk until complete screening of the DW is achieved. In the case of $ErMnO_3$, a theoretical model for DWC was already developed.[24] However, it is not applicable for LNO since an opposite experimental result was obtained (enhanced conductivity of head-to-head, not tail-to-tail DWs). Furthermore, DWC in $ErMnO_3$ requires no additional illumination. For LNO, DWC was modeled within the framework of semiconductor physics,[23] predicting an increase of the DWC over several orders of magnitude, as compared to the bulk, but once again without the requirement for any illumination. In contrast, we found that DWC could not be measured in the dark, but photoexcitation of electron-hole pairs by super-bandgap illumination is necessary to obtain a measurable DW current. This is even more remarkable as the UV light is absorbed close to the illuminated crystal surface, thus leaving most of the sample volume in the dark. The dependence of the DW current on the intensity indicates that the current does not exceed the rate of photo-excited charge carriers.

The fact that DWC in LNO was observed under UV illumination bears considerable potential for future applications since, under these terms, the DWC can be influenced on purpose via external illumination. This is all the more interesting because charged DWs can occur in any ferroelectric and photoinduced DWC may therefore not be restricted to LNO, but is likely to be found in other (single crystalline) ferroelectrics and multiferroics as well. For instance, nanocontacts built-up by conducting DWs might be employed as contact leads to nanoelectronic structures placed on top of an initially perfectly insulating ferroic single crystal, down to the molecular scale. In such a case, we benefit here from a) the nanoscale precision of placing these conductive channels by domain engineering and b) the tuneability of DWC that allows for switching and/or continuous modulation of the current, by choosing the right contact materials, sample doping and inclination angle. Furthermore, the localized transport can be elegantly combined with nanostructure self assembly at the DWs (ferroelectric lithography). The coincidence of photoinduced conductivity and photochemical surface reactivity will allow for an easy and switchable electrical contacting of such structures.

5. Conclusions

In summary, we have identified an unexpected photoinduced current along DWs in thick sc-LNO samples whereby the conductivity can be tuned by varying the inclination angle α and thus the charge density σ of the DWs. In contrast to theoretical predictions we could show that DW conductivity in LNO requires super-bandgap illumination at one of the crystal faces, whereby the strength of the DW current was found to depend on the intensity of the illumination. In the context of other investigations on DWC reported for thin oxide films, it is worth to underline that our results were obtained on thick samples and moreover from single crystalline materials constituting wide-bandgap semiconductors.

6. Experimental Section

Domain Engineering: The samples used in our experiments were congruent LNO single crystals (CLN), either undoped or doped with 1, 2, 3 and 5 mol% magnesium. All samples were prepared as *z*-cut and had thicknesses of 15 μm, 300 μm and 500 μm, respectively. Initially, all crystals were in single domain state. Electric field poling of the crystals was carried out for the fabrication of A- and B-LNO samples.[37,38] The thick samples were macroscopically contacted with liquid electrodes and partially poled by applying voltage pulses of ≈ 0.5 s duration exceeding the coercive field inside the sample resulting in quasi-stochastic domain patterns over mm^2 areas. By this, domains of different sizes between 5 and 500 μm and more or less hexagonal shapes could be generated. These domains penetrate through the whole crystal thickness and are therefore referred to as bulk domains. The domain pattern in the 15 μm thick sample was fabricated by locally applying voltage pulses (100 V, 60 s) with an AFM tip. Surface domains were prepared by UV-assisted poling.[39,40] Using this UV-technique

domains at a predefined position, with given size and shape can be generated.

PFM investigation on both *z*-faces and domain area comparison revealed that the DWs in undoped CLN samples exhibit $\alpha = 0°$ (A-LNO). The DWs in Mg-doped CLN, however, have a non-zero inclination which increases with increasing Mg-content. These DWs are positively charged, the samples therefore belong to type B-LNO ($0° < \alpha < 90°$). The inclination angle α can be reduced by heating the samples at 200 °C under ambient conditions. After annealing a 5 mol% Mg-doped B-LNO sample for 1 hour no inclination of the domain walls could be measured anymore, thus the formerly B-LNO was transformed into A-LNO.

C-LNO samples ($\alpha \approx 90°$) were prepared by heating a single domain crystal up to ≈1100 °C for 10 h, which leads to a domain inversion of half of the sample.[27] In this case a head-to-head DW forms, carrying the maximal allowed charge.

Measurement Setups: The AFM measurements were performed under ambient conditions with an AIST-NT SmartSPM 1000 scanning force microscope using an additional current amplifier. The rear face of the sample was contacted uniformly either with silver paint or with an evaporated thin metal film consisting of 1 nm Cr as adhesion layer and 10 nm Au. This metal film electrode is semitransparent for the wavelength region of interest (transmission ≈ 40%). The Pt-coated tip served as opposite electrode at the top face of the sample. For super-bandgap illumination ($\lambda < 310$ nm) UV LEDs with wavelengths of 310, 300, 270, 260 and 250 nm were used. For sub-bandgap illumination LEDs with wavelengths in the range of 320 to 400 nm were used. The maximum intensities were 12.5 μW mm^{-2}. The spectral FWHM was below 12 nm for all LEDs.

The macroscopic measurements were performed in an Oxford Instruments Optistat DN liquid nitrogen optical cryostat. An Keithley 6517B electrometer was used for the current and resistance measurements. The resolution of the electrometer is 0.1 fA and the accuracy of the setup was ±200 fA. The samples were contacted with 1 nm Cr/10 nm Au thin film circular electrodes of 2.3 mm in diameter evaporated on opposite faces of the sample. The total length of the DWs within this contact area was estimated to be ≈ 50 mm for the B-LNO sample used for the measurements. The voltage was applied to one electrode and the opposite electrode was connected to the current input of the electrometer on virtual ground. An additional guard ring prevented from surface currents. Illumination took place with a monochromatized xenon arc lamp with an spectral FWHM of 10 nm whereby the samples were illuminated under normal angle through the electrode connected to the electrometer. For the C-LNO samples the resistance was measured in a simple two point geometry.

Supporting Information

Supporting Information is avialable from the Wiley Online Library or from the author.

Acknowledgements

Financial support by the Deutsche Forschungsgemeinschaft (DFG) within the research training group 1401/1: "Nano- and Biotechnologies for Packaging of Electronic Systems" is gratefully acknowledged.

Received: April 27, 2012
Published online: May 31, 2012

[1] R. Waser, A. Rüdiger, *Nat. Mater.* **2004**, *3*, 81.
[2] R. E. Newnham, S. Miller, L. E. Cross, T. W. Cline, *Phys. Status Solidi A* **1975**, *38*, 69.
[3] L. E. Myers, R. C. Eckardt, M. M. Fejer, R. L. Byer, W. R. Bosenberg, J. W. Pierce, *J. Opt. Soc. Am. B* **1995**, *12*, 2102.
[4] Y. Cho, S. Hashimoto, N. Odagawa, K. Tanaka, Y. Hiranaga, *Appl. Phys. Lett.* **2005**, *87*, 232907.
[5] H. Chaib, T. Otto, L. M. Eng, *Phys. Status Solidi B* **2002**, *233*, 250.
[6] H. Béa, P. Paruch, *Nat. Mater.* **2009**, *8*, 16869.
[7] C.-L. Jia, S.-B. Mi, K. Urban, I. Vrejoiu, M. Alexe, D. Hesse, *Nat. Mater.* **2008**, *7*, 57.
[8] D. Lee, H. Xu, V. Dierolf, V. Gopalan, S. R. Phillpot, *Appl. Phys. Lett.* **2011**, *98*, 092903.
[9] C. Loppacher, F. Schlaphof, S. Schneider, U. Zerweck, S. Grafström, L. M. Eng, A. Roelofs, R. Waser, *Surf. Sci.* **2003**, *483*, 532.
[10] Y. L. Wang, A. K. Tagantsev, D. Damjanovic, N. Setter, *Appl. Phys. Lett.* **2007**, *91*, 062905.
[11] J. N. Hanson, B. J. Rodriguez, R. J. Nemanich, A. Gruverman, *Nanotechnology* **2006**, *17*, 4946.
[12] A. Haussmann, P. Milde, C. Erler, L. M. Eng, *Nano Lett.* **2009**, *9*, 763.
[13] M. Calleja, M. T. Dove, E. K. H. Saljé, *J. Phys.: Condens. Matter* **2003**, *15*, 2301.
[14] A. Aird, E. K. H. Saljé, *J. Phys.: Condens. Matter* **1998**, *10*, L377.
[15] A. Aird, E. K. H. Saljé, *Eur. Phys. J. B* **2000**, *15*, 205.
[16] J. Seidel, L. W. Martin, Q. He, Q. Zhan, Y.-H. Chu, A. Rother, M. E. Hawkridge, P. Maksymovych, P. Yu, M. Gajek, N. Balke, S. V. Kalinin, S. Gemming, F. Wang, G. Catalan, J. F. Scott, N. A. Spaldin, J. Orenstein, R. Ramesh, *Nat. Mater.* **2009**, *8*, 229.
[17] S. Farokhipoor, B. Noheda, *Phys. Rev. Lett.* **2011**, *107*, 127601.
[18] J. Seidel, P. Maksymovych, Y. Batra, A. Katan, S.-Y. Yang, Q. He, A. P. Baddorf, S. V. Kalinin, C.-H. Yang, J.-C. Yang, Y.-H. Chu, E. K. H. Salje, H. Wormeester, M. Salmeron, R. Ramesh, *Phys. Rev. Lett.* **2010**, *105*, 197603.
[19] J. Guyonnet, I. Gaponenko, S. Gariglio, P. Paruch. *Adv. Mater.* **2011**, *23*, 5377.
[20] S. Y. Yang, J. Seidel, S. J. Byrnes, P. Shafer, C.-H. Yang, M. D. Rossell, P. Yu, Y.-H. Chu, J. F. Scott, J. W. Ager, III, L. W. Martin, R. Ramesh, *Nat. Nanotechnol.* **2010**, *5*, 143.
[21] J. Seidel, D. Fu, S.-Y. Yang, E. Alarcón-Lladó, J. Wu, R. Ramesh, J. W. Ager, *Phys. Rev. Lett.* **2011**, *107*, 126805.
[22] M. Y. Gureev, A. K. Tagantsev, N. Setter, *Phys. Rev. B* **2011**, *83*, 184104.
[23] E. A. Eliseev, A. N. Morozovska, G. S. Svechnikov, V. Gopalan, V. Y. Shur, *Phys. Rev. B* **2011**, *83*, 235313.
[24] D. Meier, J. Seidel, A. Cano, K. Delaney, Y. Kumagai, M. Mostovoy, N. A. Spaldin, R. Ramesh, M. Fiebig, *Nat. Mater.* **2012**, *11*, 284.
[25] W. Wu, Y. Horibe, N. Lee, S.-W. Cheong, J. R. Guest, *Phys. Rev. Lett.* **2012**, *108*, 077203.
[26] B. A. Strukov, A. P. Levanyuk, *Ferroelectric Phenomena in Crystals*, Springer, New York **1998**.
[27] V. D. Kugel, G. Rosenman, *Appl. Phys. Lett.* **1993**, *62*, 2902.
[28] S. V. Kalinin, B. J. Rodriguez, S. Jesse, E. Karapetian, B. Mirman, E. A. Eliseev, A. N. Morozovska, *Annu. Rev. Mater. Res.* **2007**, *37*, 189.
[29] L. M. Eng, H.-J. Güntherodt, G. A. Schneider, U. Köpke, J. Muñoz Saldaña, *Appl. Phys. Lett.* **1999**, *74*, 233.
[30] T. Volk, M. Wöhlecke, *Lithium Niobate: Defects, Photorefraction and Ferroelectric Switching*, Springer, Berlin, Germany **2008**.
[31] A. C. Muir, C. L. Sones, S. Mailis, R. W. Eason, T. Jungk, A. Hoffman, E. Soergel, *Opt. Express* **2008**, *16*, 2336.
[32] Note that illuminating LNO with super-bandgap light is fundamentally different to the sub-bandgap excitation of impurities such as Fe^{2+} as treated extensively for holographic investigations in the literature.[28]
[33] M. Abplanalp, L. M. Eng, P. Günter, *Appl. Phys. A* **1998**, *66*, S231.

[34] K. Buse, *Appl. Phys. B* **1997**, *64*, 273.
[35] B. Kohlrausch, *Ann. Phys.* **1854**, *167*, 179.
[36] G. Williams, D. C. Watts, *Trans. Faraday Soc.* **1970**, *66*, 80.
[37] G. Rosenman, P. Urenski, A. Agronin, Y. Rosenwaks, M. Molotskii, *Appl. Phys. Lett.* **2003**, *82*, 103.
[38] D. Li, D. A. Bonnell, *Annu. Rev. Mater. Res.* **2008**, *38*, 351.
[39] M. Müller, E. Soergel, K. Buse, *Appl. Phys. Lett.* **2003**, *83*, 1824.
[40] T. Volk, M. Wöhleke, N. Rubinina, in *Photorefractive Materials and Their Applications 2* (Eds: P. Günter, J. P. Huignard), Springer Science + Business Media, New York **2007**, Ch. 6.